Dyes and Pigments 132 (2016) 291–305

Contents lists available at ScienceDirect

Dyes and Pigments

journal homepage: www.elsevier.com/locate/dyepig

Photoluminescent discotic liquid crystals derived from tris(*N*-salicylideneaniline) and stilbene conjugates: Structure–property correlations

Ammathnadu S. Achalkumar [b, *], B.N. Veerabhadraswamy [a], Uma S. Hiremath [a], Doddamane S. Shankar Rao [a], Subbarao Krishna Prasad [a], Channabasaveshwar V. Yelamaggad [a, **]

[a] Centre for Nano and Soft Matter Sciences, Jalahalli, Bangalore 560 013, India
[b] Department of Chemistry, Indian Institute of Technology Guwahati, Guwahati 781039, Assam, India

ARTICLE INFO

Article history:
Received 16 February 2016
Received in revised form
19 April 2016
Accepted 9 May 2016
Available online 10 May 2016

Keywords:
Stilbene
OLEDs
Liquid crystals
Columnar phase
Glassy state

ABSTRACT

Luminescent discotic liquid crystals based on tris(*N*-salicylideneaniline)s [TSANs] bearing *trans*-stilbene fluorophores have been synthesized. Their mesomorphic and photophysical properties were studied. These TSANs existing in the form of C_{3h} and C_s geometrical isomers of the keto-enamine tautomer self-assemble to form the columnar phase and exhibit fluorescence both in solution and mesophase states. These columnar mesophases also exhibit frozen (glassy) columnar phase, which ensures preserved fluorescence intensity, defect free alignment and simultaneous restriction on the motion of ionic impurities. These features make them promising candidates for the use in organic light emitting diodes, particularly as emissive layers. This study also led to an understanding about the dependence of their mesomorphism (mesophase type, stability and thermal range) and photophysical features on the number and pattern of their peripheral substitution, in comparison to the analogous columnar liquid crystalline TSANs reported earlier.

1. Introduction

The discovery of electroluminescence over five decades ago in organic semiconductors [1] gave rise to a thriving and promising research area of organic light emitting diodes (OLEDs). OLEDs, essentially comprising the organic emitter layer, have been regarded as the forerunner of modern advanced display technology. Over the years it is well demonstrated that OLED devices have distinct advantages [2,3] over their nearest competitors like liquid crystal displays (LCDs) or cathode ray tube (CRT) devices. They can be effectively used in fabricating micro- to large-size flat (stiff) panel displays, flexible plastic displays, screens fixed into clothes/wall hangings, etc. The brighter and higher quality of image, better contrast, tunability of the color, reduced viewing angle problem, non-requirement of backlighting, and more importantly the lower power consumption make OLEDs even more attractive and hopeful media in display screens. However, all such important features of OLED panels vitally depend on the various physical properties of organic material(s) used. Such molecules comprising chromophores basically absorb incident energy and emit light in the visible regime. The color of the emitted light (red, green, and blue) largely depends on the composition of the material. Consequently, the field, involving molecular design and synthesis, has well-broadened to include every class of materials *viz.*, small molecules, oligomers, organometallics, polymers etc. [4].

Discotic liquid crystals (discotics), generally formed by covalently linking several paraffinic chains to a disk-like (flat) aromatic central ring, fall under the class of small molecules. Generally, owing to strong noncovalent interactions among aromatic cores ($\pi-\pi$ stacking), they self-assemble to form fluid columnar (Col) structures characterized by indefinitely long molecular columns aggregating into two-dimensional (2D) lattices of varying symmetries. The innermost aromatic ring of a disc-like molecule acts as a conducting unit, while peripheral paraffinic tails act as an insulator. Consequently, the assembly of such molecules into 1D Col

* Corresponding author.
** Corresponding author.
E-mail addresses: achalkumar@iitg.ernet.in (A.S. Achalkumar), yelamaggad@cnsms.com, yelamaggad@gmail.com (C.V. Yelamaggad).

http://dx.doi.org/10.1016/j.dyepig.2016.05.010
0143-7208/

stacks assists smooth charge-transport along columns than across the columns; thus, they act as molecular wires. Columnar phases are the latest entrants in the field of OLEDs. In fact, the 1D columnar arrays are the ideal alternatives for organic single crystals or amorphous conjugated polymers which are finding applications in OLEDs [5–8], solar cells [9–11], and field effect transistors [12–14]. This increasing acceptance of Col phases in such devices, arises from their inherent properties such as its anisotropic conductivity, control over the molecular order, solution processability and structural self healing. Most importantly all these properties can be tailored by careful molecular engineering which is difficult in the case of single crystals or conjugated polymers. In the case of OLEDs, Col phases are mainly used as hole carrying or electron carrying or emissive layers. Majority of disc-like mesogens like triphenylene, dibenzopyrene, and hexabenzocoronene etc. comprise electron-rich (donor) aromatic cores [15–19] and are known as good hole transporters, whereas DLCs derived from electron-deficient systems are limited in number. There are few examples like coronene derivatives substituted with electron withdrawing groups or systems based on heterocyclic cores such as triazines, quinoxalines [15–19], hexaazatriphenylene [20] and hexaazatrinaphthylene [21,22] etc. Unfortunately, most self-assembling aromatic systems because of their poor emissive nature cannot be used as emissive layers in OLEDs. Thus many research groups are working on the design of columnar luminescent LCs which guarantee the orientationally ordered luminophores [23–29]. Material chemists are in the hot pursuit of molecules which combine the hole carrying, electron carrying and emissive features in a single molecule to avoid the complexities and associated problems in the fabrication of OLEDs with enhanced efficiencies [30].

Tris(*N*-salicylideneaniline)s (TSANs) [31–42], relatively a new class of discotics are encouraging as they can be easily tailored to introduce features like luminescence, self-organizing ability, molecular recognition etc. [31–42]. McLachalan et al., reported that this new class of molecules are existing as an inseparable mixture of C_{3h} and C_s symmetric regioisomers of the keto-enamine tautomer [31]. With the introduction of peripheral alkyl tails, the same compounds stabilized Col phase/s [33]. Further studies revealed the promising inherent luminescence behavior of these compounds [34–39]. Lee et al., have shown that intelligently modified the structure of TSANs, which led to the self-assembly of C_{3h} isomers in such a way that it enhanced fluorescence efficiency in solutions [40–42]. It is also postulated that the columnar organization of discotic molecules with fluorophores is beneficial for the energy transfer because of the effective Forster mechanism [43]. As part of our ongoing research in luminescent LCs and our previous work on TSANs we wanted to incorporate various fluorophores. We succeeded in obtaining blue light emitting DLCs, by incorporating an oxadiazole moiety in the molecular structure of TSANs [37]. Thus we thought of introducing other fluorophores into the molecular structure of TSANs. It seemed that *trans*-stilbene chromophore was an ideal option to enhance the fluorescence property of TSANs [38], because of their interesting properties [44,45]. Apart from their commercial use as optical brighteners and laser dyes, their inclination for charge carrier mobility and electroluminescence has found applications in OLEDs [46–48], field effect transistors and photovoltaic cells [49]. Initial study in this direction is reported in our earlier communication [38], while in this paper we are presenting yet another three set of stilbene-TSANs to account for an in-depth study. Precisely, in this work, we have designed and synthesized three types of luminescent TSANs, labeled as **Ia**–**b**, **IIa**–**b** and **IIIa**–**d** (Fig. 1), bearing *trans*-stilbene unit where the length, number and pattern of substitution of exterior alkyl chains have been varied. These new TSANs were targeted and prepared primarily to compare their mesomorphism and photophysical behavior with those of the lower homologues of TSANs **Ia**–**b** and **IIa**–**b** (Fig. 1) reported previously in the form of a communication [38]. It may be ideal to mention here that the design and synthesis of materials herein dealt with are inspired by the potential applications of disk-like LCs; however, detailed experiments dealing with technological aspects do not fall within the scope of our work described herein.

2. Results and discussion

2.1. Synthesis and molecular structural characterization

The target stilbene-based TSANs were synthesized as outlined in Scheme 1. 1,3,5-Triformyl phloroglucinol (**1**) was synthesized by Duff's formylation as reported earlier [31,33]. As can be seen in Scheme 1, 1,4-nitrotoluene was subjected to benzylic bromination by refluxing a solution of *N*-bromosuccinimide (NBS) in anhydrous carbon tetrachloride with azobisisobutyronitrile (AIBN) as a radical initiator to obtain 4-nitrobenzyl bromide (**2a**). This compound was reacted with triethyl phosphite following Michaelis–Arbuzov phosphonate synthesis procedure, to obtain diethyl 4-nitrobenzylphosphonate (**2b**). The requisite 3,4-dialkoxybenzaldehydes (**3a**–**b**) were prepared in quantitative yields by O-alkylation of 3,4-dihydroxybenzaldehyde with various alkyl bromides following Williamson's ether synthesis protocol. The Wittig–Horner reaction of these benzaldehydes **3a**–**b** with the diethyl ester **2b** in the presence of lithium diisopropyl amide (LDA) as a base in tetrahydrofuran (THF) at low temperature (−78 °C) furnished nitro compounds **4a**–**b** in good yields. These nitro products were converted to corresponding amines **5a**–**b** by selective reduction of nitro group using a mixture of indium powder and hydrochloric acid in THF. On the other hand, the trialkoxy stilbene amines **10a**–**b** and **13a**–**d** were prepared starting from 3,4,5-trialkoxybenzaldehydes (**8a**–**b**) or 2,3,4-trialkoxybenzaldehydes (**11a**–**d**) respectively, by following the synthetic steps as described for the amines **5a**–**b**. 3,4,5-Trialkoxybenzaldehydes (**8a**–**b**) were synthesized, by the oxidation of (3,4,5-tris(alkoxy) phenyl)methanol (**7a**–**b**) using pyridinium chlorochromate (PCC), while compounds **7a**–**b** were obtained by the lithium aluminium hydride (LAH) mediated reduction of ethyl 3,4,5-trialkoxybenzoates (**6a**–**b**). Finally, the aminostyryl compounds **5a**–**b** or **10a**–**b** or **13a**–**d** were reacted with 1,3,5-triformyl phloroglucinol in refluxing ethanol to obtain the respective target molecules **Ia**–**b**, **IIa**–**b** and **IIIa**–**d** in almost quantitative yields.

All the target molecules, **Ia**–**b**, **IIa**–**b** and **IIIa**–**d**, existed in the form of an inseparable mixture of C_{3h} and C_s geometrical isomers of keto-enamine tautomer as evidenced by ^{1}H and ^{1}H–^{1}H COSY NMR spectra. In fact, as expected, the NMR spectra of TSANs **Ia**–**b** and **IIa**–**b** were found to be identical to the spectra of their lower homologues substituted with *n*-octyloxy, *n*-decyloxy and *n*-dodecyloxy terminal chains [38], which are hereafter, respectively, refer to as **I-C8**, **I-C10** & **I-C12** and **II-C8**, **II-C10** & **II-C12** for the sake of convenience and discussion. In particular, the proton spectra showed multiple peaks between δ 8.7–8.9 and δ 13.1–13.5 due to the resonance of enamine and 2°-amine protons respectively, and their coupling. As can be seen (SI), the region *viz.*, δ 13.1–13.5 consisted of four doublets due to the resonance of an amine proton (H_e) of C_{3h} isomer and three analogous protons (H_f, H_g and H_h) of C_s isomer. The enamine region *viz.*, δ 8.7–8.9 also consisted of four doublets, which are due to the resonance of a proton (H_a) of C_{3h} isomer and three protons (H_b, H_c and H_d) of C_s isomer. In principle, the measure of the integration of H_e against H_f, H_g and H_h of amine protons or H_a *vs* H_b, H_c and H_d of enamine protons can be considered to calculate the ratio of two isomers. In this discussion, we considered amine protons for estimating the ratio of the two

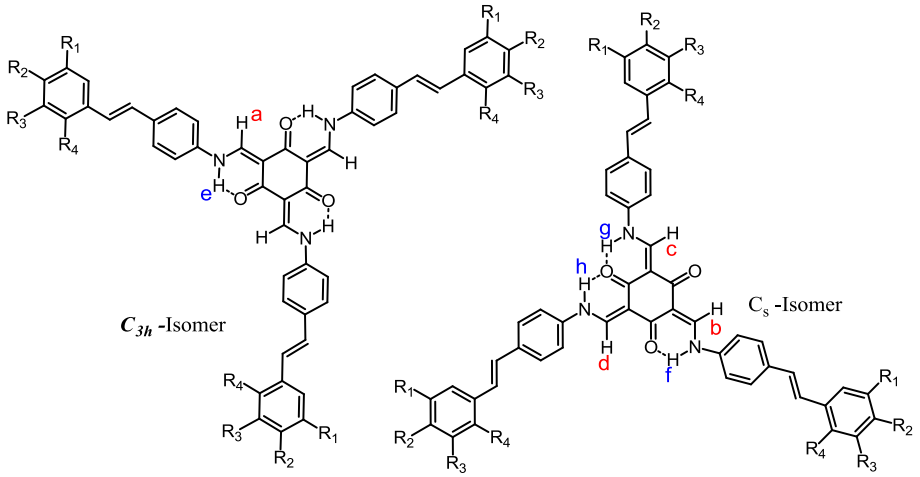

Series-I
Ia : $R_1 = R_2 = n\text{-}OC_{16}H_{33}$, $R_3 = R_4 = H$
Ib : $R_1 = R_2 = 3,7\text{-Dimethyloctyloxy}$, $R_3 = R_4 = H$
I-C8 : $R_1 = R_2 = n\text{-}OC_8H_{17}$, $R_3 = R_4 = H$
I-C10 : $R_1 = R_2 = n\text{-}OC_{10}H_{21}$, $R_3 = R_4 = H$
I-C12 : $R_1 = R_2 = n\text{-}OC_{12}H_{25}$, $R_3 = R_4 = H$

Series-II
IIa : $R_1 = R_2 = R_3 = n\text{-}OC_{16}H_{33}$; $R_4 = H$
IIb : $R_1 = R_2 = R_3 = 3,7\text{-Dimethyloctyloxy}$; $R_4 = H$
II-C8 : $R_1 = R_2 = R_3 = n\text{-}OC_8H_{17}$, $R_4 = H$
II-C10 : $R_1 = R_2 = R_3 = n\text{-}OC_{10}H_{21}$, $R_4 = H$
II-C12 : $R_1 = R_2 = R_3 = n\text{-}OC_{12}H_{25}$, $R_4 = H$

Series-III
IIIa : $R_2 = R_3 = R_4 = OC_8H_{17}$; $R_1 = H$
IIIb : $R_2 = R_3 = R_4 = OC_{12}H_{25}$; $R_1 = H$
IIIc : $R_2 = R_3 = R_4 = OC_{16}H_{33}$; $R_1 = H$
IIId : $R_2 = R_3 = R_4 = OC_{18}H_{37}$; $R_1 = H$

Fig. 1. Molecular structures of new and analogous luminescent discotic TSANs.

isomers, because of the ease in estimation (Scheme 1). $^1H-^1H$ COSY NMR spectra confirmed the coupling between the enamine and the NH protons. Furthermore, the strong coupling ($^3J_{HH}$ ~13 Hz) [50] explains the localization of the NH proton. The proton NMR spectra for the materials did not show any signals corresponding to *cis* isomeric protons, demonstrating that the stilbene units are in the desired *trans* form, which is the expected outcome of the Wittig–Horner–Emmons method. These *trans* olefinic protons were distinguished as doublets in the downfield region with a large coupling constant (J_{HH} ~16 Hz). In the case of **Ia**–**b** and **IIa**–**b** series, two doublets corresponding to these olefinic protons resonate at around δ 7 and 7.05, while in the case of **IIIa**–**d** series they appear at δ 7 and 7.4. Molecular structures were further confirmed by IR, UV–vis spectroscopy, FAB+ mass spectrometry and elemental analysis.

2.2. Mesomorphic behavior

The phase behavior of the synthesized TSANs were established with the aid of polarizing optical microscopy (POM), differential scanning calorimetry (DSC) and X-ray diffraction (XRD) studies; in fact, XRD data have also been obtained, as representative cases, for TSANs **I-C8** and **II-C8**. The detailed investigations of the mesomorphic behavior of these three series of compounds are presented in the sections to follow. The data obtained from these studies are summarized in Tables 1 and 2 and Fig. 2.

2.2.1. Series-I

The thermal behavior of the two newly synthesized compounds were examined and compared with that of previously reported lower homologues **I-C8**, **I-C10** and **I-C12** (Table 1 and Fig. 2). All the homologues of this series were liquid crystalline; exhibiting enantiotropic Col phase as per the POM observation. The crystalline sample, **Ia** with a melting temperature of 81 °C changes into Col mesophase which stays up to ~224 °C, before transforming into isotropic state. On cooling the isotropic liquid, a texture, which is a combination of small focal conics, interspersed with linear birefringent defects, is observed. This pattern grows from an initially homeotropic dark field of view, which is commonly attributed for the Col_h phase [56]. Further cooling leads to large pseudo focal conics covering the whole field of view (Fig. 3a). Finally the mesophase crystallized at 29 °C. XRD studies confirm the D_{6h} (hexagonal) symmetry of the mesophase. As can be seen in Fig. 3b, the intensity *vs* 2θ profile extracted from the 2D XRD pattern displays two sharp Bragg peaks, an intense one (100) at a spacing 42.21 Å and a relatively weak one (110) with a *d* spacing of 24.42 Å. Additionally a diffused peak in the wide angle was observed with a spacing of 4.7 Å. The first two peaks in the small angle were in the ratio of 1:0.58, which proves that the mesophase under investigation is Col_h, with the cell parameter $a = 43.74$ Å. The XRD pattern obtained at low temperatures (100 °C) was qualitatively similar but an additional diffuse peak corresponding to an intra columnar core–core stacking distance of 3.46 Å was also observed.

The next compound **Ib** comprising branched peripheral chains, showed an enantiotropic columnar phase with much reduced transition temperatures when compared to the analogous values obtained for compound **Ia** or other members of the series. Needless to say, in this compound there is more fluidic disorder as it possesses branched alkyl chains at the peripheral region [57–59]. The thermal behavior of this compound also approves with the fact that the presence of branched alkyl chains widen the mesophase width, without altering the mesophase type [5–14,57–59].

The observed optical pattern for the mesophase was identical to the one seen for **Ia** and it is reasonable to adjudge that compound **Ib** also stabilizes the Col_h phase (Fig. 4a). Notably, the Col phase formed upon melting the crystalline sample, does not crystallize as

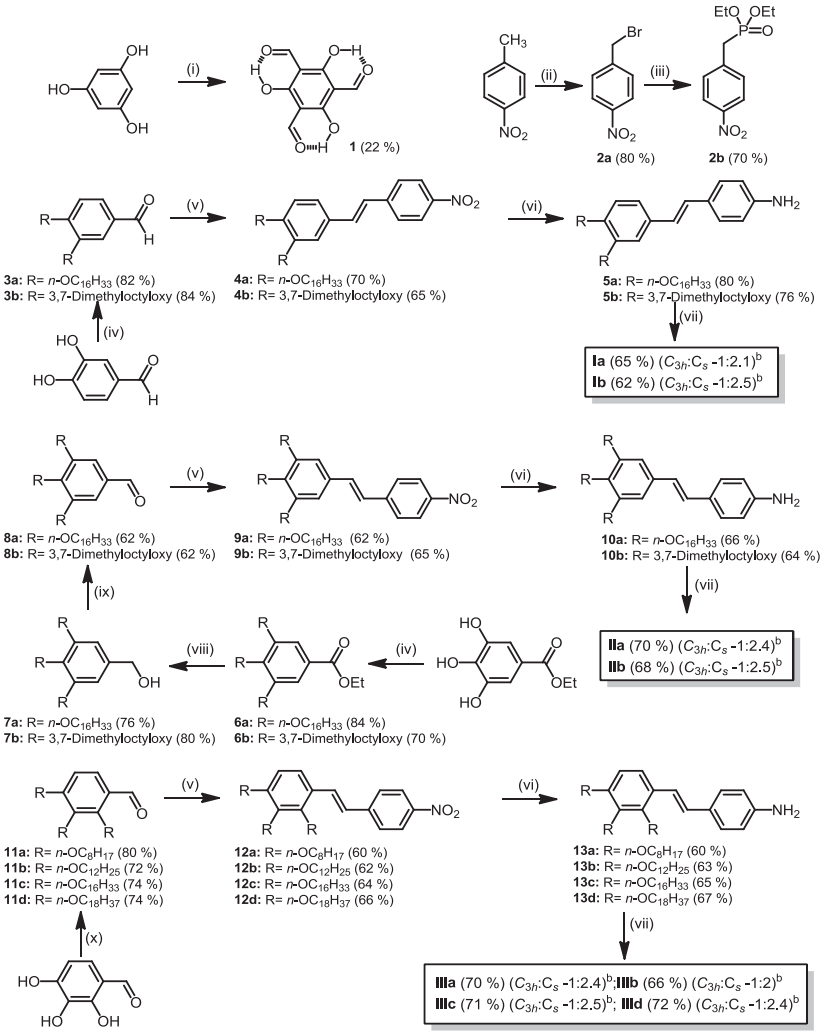

[a]**Reagents and conditions**(i) Hexamine, CF_3COOH, 100 °C, 5 h, 3N HCl, 100 °C ; (ii) NBS, AIBN, CCl_4, 100 °C, 6 h; (iii) Triethyl phosphite, 130 °C, 6 h; (iv) 3,7-Dimethyloctylbromide / *n*-hexadecylbromide, anhydrous K_2CO_3, DMF, 80 °C, 17 h; (v) **2b**, LDA, THF, -78 °C to rt, 12 h; (vi) Indium powder, Conc. HCl, THF (1:9), rt, 2 h; (vii) **1,** ethanol, 80 °C, 6 h. (viii) LAH, THF, 0 °C to rt, 12 h; (ix) PCC, DCM, rt, 1 h; (x)1-Bromooctane/1-bromodecane/1-bromohexadecane /1-bromooctadecane, anhydrous K_2CO_3, DMF, 80 °C, 17 h.[b]The ratio of C_{3h} and C_s isomers was determined by comparing the integral areas of amine protons H_e (C_{3h} isomer) *vs* H_f , H_g and H_h(C_s isomer) in ^{1}H NMR.

Scheme 1. [a]Synthesis of stilbene-based TSANs.

evidenced by the observation that the texture remains unchanged for a long time. Further, no exothermic or endothermic peaks were seen in the first cooling or second heating DSC profiles respectively. The XRD studies carried out at higher temperature (Fig. 4b) and room temperature (RT) suggested that the compound stabilized Col_h phase. An identical behavior was noticed for lower homologues reported earlier stabilizing Col_h mesophase as evidenced by the POM, DSC and XRD investigations. In this series, on increasing the chain length, the mesophase range seems to increase marginally in heating cycle (Fig. 2a), while the compound with branched chain showed a reduced mesophase range (Fig. 2d). Compound **I-C8** also exhibits Col_h phase as evidenced by the XRD studies. The absence of multiple reflections in the low angle region of the XRD pattern could be assigned to a minimum in the form factor. Though, the existence of a single (100) peak does not allow the unambiguous assignment of the Col_h phase, the situation is similar to several previous reports, wherein such an observation coincides with a hexagonal columnar arrangement [43,51–55].

2.2.2. Series-II

When compared to TSANs **Ia** and **Ib**, discotics **IIa** and **IIb** showed a drastic reduction in the melting temperature. Increase in the number of flexible tails from six to nine enhanced the mesophase range. Increase in the chain length of the peripheral tails showed a gradual decrease in the melting and clearing temperatures. Branching in the peripheral chains (compound **IIb**) does not show the pronounced effect as it is in the case of compound **Ib**. It may also be noted that, although not related directly, the short armed TSANs with six peripheral tails exhibit lower melting temperatures when compared to their analogous compounds comprising nine alkoxy tails [33,36]. This behavior is contrary to the thermal behavior of stilbene based TSANs (Series **I** and **II**). In this series, on increasing the chain length, both the clearing temperature and the mesophase range seems to decrease, as illustrated in Fig. 2b and e.

Table 1
Phase transition temperatures (°C)[a] and corresponding enthalpies (J/g) of **Ia–e** series.

Entry	Phase sequence	
	Heating	Cooling
Series-I		
I-C8	Cr 125.6 [20.2] Col_h 218.4 [1] I	I 214.9 [0.9] Col_h 1.3 [0.6] Cr
I-C10	Cr 111.2 [8.1] Col_h 229.2 [1.2] I	I 226.6 [1][b] Col_h
I-C12	Cr 107 [35.3] Col_h 239.5 [1.7] I	I 237 [1.5][b] Col_h
Ia	Cr 80.7 [13.5] Col_h 223.5 [1.3] I	I 220.3 [1.2] Col_h 29.4 [13.2] Cr
Ib	Cr 65.7 [1.6] Col_h 192 [1.1] I	I 188.2 [1.3][b] Col_h
Series-II		
II-C8	Cr 72.4 [1.4] Col_h 240.4 [1.1] I	I 236.3 [1.1][b] Col_h
II-C10	Cr 70.1 [1.4] Col_h 226.2 [1.4] I	I 220 [1.2][b] Col_h
II-C12	Cr 66.5 [1.5] Col_h 199.5 [1.6] I	I 196.5 [1.4][b] Col_h
IIa	Cr 41.5 [24.9] Col_h 140.2 [0.6] I	I 135.5 [0.6][b] Col_h
IIb	Cr 65.7 [0.9] Col_h 193.9 [1.3] I	I 190 [1.2][b] Col_h
Series-III		
IIIa	Cr 117.3 [6.7] I	I 97.2 [1.7] Col_{ob} 71.5 [0.5] Cr
IIIb	Cr 95.7 [7.2] Col_h 114.3 [1.1] I	I 106.6 [0.5] Col_h 60 [0.3] Cr
IIIc	Cr 77.2 [0.4][c] Col_r 83.5 [1.9] I	I 78.7 [1] Col_r 72.9 [1.9] Cr
IIId	Cr 76.3 [10.6] I	I 56.2 [37] Cr

[a] Peak temperatures in the DSC thermograms obtained during the first heating and cooling cycles at 5 °C/min.
[b] The mesophase is not crystallizing up to −60 °C. Cr = Crystal; Col_h = Hexagonal columnar phase; I = Isotropic liquid.
[c] Cr–Cr transition is observed at 107.1 [0.4], 69.2 [13.8] and 57.2 [12.7] for **IIIa**, **IIIc** and **IIId** respectively in the first heating cycle.

Firstly, let us discuss the phase behavior of compound **IIa**. This TSAN sandwiched between a glass slide and coverslip, on heating, melts into a mesophase at about 42 °C having a non-specific textural pattern; on further heating it transforms into isotropic liquid at ~140 °C. On cooling from the isotropic phase, a columnar (Col) phase appears with the texture consisting of a combination of mosaics with linear birefringent defects and homeotropic regions (Fig. 5a). The presence of some homeotropic domains strongly suggests that the phase is hexagonal columnar (Col_h). On further cooling, the compound did not crystallize but appeared to form a glass nearing about 60 °C. The signatures in DSC thermograms due to all of the above phase transitions, except for Col-glass, were obtained. This Col phase was studied further by XRD at two different temperatures *viz.* 120 °C and 60 °C, in order to ascertain its structure. As expected, both the diffractograms were found to be identical and as a representative case we explain the diffraction pattern obtained at 60 °C. 1D intensity *vs* 2θ profile obtained at 60 °C has been shown in Fig. 5b. A diffuse peak in the wide-angle region with $d \approx 4.5$ Å is seen, which can be attributed to the liquid like (short-range) order of the peripheral alkoxy tails. A prominent peak in the wide-angle region corresponding to core–core stacking was observed in the low temperature diffraction pattern with a *d* spacing of 3.6 Å. In addition, a sharp reflection was observed in the low angle regions with the spacing being 46.2 Å. Additionally the low angle region had peaks corresponding to the *d* spacings of 26.8 Å, 17.47 Å and 11.62 Å with Miller indices (100), (110) and (210). These *d* spacings were in a ratio of 1:0.58:0.38, which corresponds to Col_h phase. Apparently, this was similar to the high temperature diffraction pattern obtained at 120 °C (Table 2 and SI), apart from the increase in the lattice parameter *a* from 49.8 Å to 53.4 Å, which can be attributed to the stretching of the peripheral alkoxy chains. The mesophase gets freezed on further cooling which was also confirmed by the DSC scans. Since the core–core stacking distance was obtained from the second diffused peak in all the diffractograms of compound **IIa**, we could calculate the lattice parameters (Table 2). For example, if we consider the X-ray diffractogram for compound **IIa** at 60 °C (Table 2 and SI), the calculated lattice parameter $a = 49.8$ Å, which is 26% less than the actual molecular diameter calculated. This may be due to the interdigitation of peripheral alkyl chains. Since the core–core distance is known, *i.e.* $c = 3.61$ Å we could calculate lattice area $S = 2466$ Å^2, lattice volume $V = 8889.3$ Å^3 and number of molecules within the columnar slice $Z = 1.84$. The value of Z which is approximately nearer to two, which means it's almost two molecules are forming a disc of the individual column. Similar values have been observed for compounds (Table 2) **Ia**, **Ib**, **IIa** and **IIb**, which exhibit Col_h phase with prominent core–core stacking distance. Even for compound **IIIa**, which exhibit columnar oblique (Col_{ob}) phase (which we discuss in later sections) the value of Z was found to be slightly more than two. This observation is common in the case of polycatenars [63] but not common in discotics and star-shaped molecules. Lehmann et al. showed that wedge shaped stilbenoid dendrons stabilized Col_h phase by the proper control of dipole or push–pull character of the central unit [45]. They proposed the packing of four dendron units to form a columnar slice with their dipoles arranged in antiparallel orientation.

We are proposing a preliminary model to explain the value of Z in the present work, as in the following. In the case of TSANs the central core with three ketone groups have three dipoles, where the negative end is pointed towards the oxygen atom. It should be noted that these three ketone groups are in conjugation with three enamine groups. Thus the next neighboring molecule may stack in such a way so as to avoid repulsion from the partial negative charge located on oxygen atom. In other words, the next molecule has to be rotated 60° with respect to the first molecule. Altogether this will help in the close packing of these molecules in a unit cell. This arrangement does not alter the molecular diameter as they are stacking one above the other. The planarity of the central core is well established due to the intramolecular H-bonding between the amine and ketone groups. As a result almost two molecules are packed in a unit cell. These individual discs are arranged in a hexagonal array as shown in Fig. 6. The observed decrease in the value of lattice parameter '*a*' with respect to molecular diameter is explained by the interdigitation of peripheral alkyl tails as shown in Fig. 6. It is interesting to note that lower homologues **II-C8**, **II-C10**, **II-C12** and branched chain derivative **IIb** also exhibited Col_h phase and an ability to freeze into glassy structure. The branched chain analogue **IIb** showed a higher melting and clearing point when compared to compound **Ib**. The compound **IIb**, when compared to **II-C8** which is the straight chain analogue; did not show a huge decrease in the melting temperature as in the case of **Ib** with respect to **I-C8** (60°). In other words, the contrasts in the melting/isotropization temperatures are apparent for compounds **Ib** & **IIb** and **Ia** & **IIa**.

2.2.3. Series-III

The general trend in thermal behavior of these three TSANs seems to be different from their positional isomeric analogues, the series **II** of compounds. In general, these TSANs show lower transition temperatures but seem to disfavor the mesomorphism. For example, the first member of the series *viz.* **IIIa** comprising three *n*-octyloxy tails at 2, 3 and 4 positions of the outermost peripheral benzene ring displays a monotropic mesophase, as was evidenced by the observation of textural pattern (Fig. 7a).

In comparison, its positional isomer **II-C8** displays an enantiotropic Col_h phase that exists for a wide thermal range (Table 1 and Fig. 2). Whereas, the compound **IIIb** having nine *n*-dodecyloxy peripheral tails display an enantiotropic mesophase; however, unlike in **II-C12**, the mesophase exists for short thermal range. Compound **IIIc** with nine hexadecyloxy chains also exhibits an enantiotropic Col phase but for a short range. Further increase in the chain length to octadecyloxy turns the compound **IIId** crystalline. It is interesting to note that first three liquid crystalline

Table 2
The results of (*hkl*) indexation of XRD profiles of the compounds at a given temperature (*T*) of mesophases.[a]

Compounds (D/Å)	Phase (*T*/°C)	d_{obs} (Å)	d_{cal} (Å)	Miller indices *hkl*	Lattice parameters (Å), lattice area *S* (Å^2), molecular volume *V* (Å^3), number of molecules in a unit cell *Z*[c]
I-C8 (45.85)	Col_h (160)	35.87	35.87	100	*a*: 41.41
		4.6 (h_a)			*S* = 1485.4
Ia (62.62)	Col_h (210)	42.21	42.21	100	*a*: 48.74
		24.42	24.37	110	*S* = 2057.2
		4.72			
		(h_a)			
	Col_h (100)	45.62	45.61	100	*a*: 52.67
		26.43	26.33	110	*c* = 3.46
		11.88[b]			*S* = 2402.26
		4.57			*V* = 8312.3
		(h_a)			*Z* = 2.29
		3.46 (h_c)			
Ib (46.85)	Col_h (180)	36.23	36.23	100	*a*: 41.84
		21.23	20.92	110	*c* = 3.71
		18.44	18.12	200	*S* = 1516.04
		13.73	13.70	210	*V* = 5620.86
		12.67[b]			*Z* = 1.99
		5.04			
		(h_a)			
		3.71 (h_c)			
	Col_h (24)	36.77	36.77	100	*a*: 42.46
		18.64	18.39	200	*c* = 3.66
		13.78	13.9	210	*S* = 1561.53
		12.62	12.26	300	*V* = 5714.84
		4.74			*Z* = 2.02
		(h_a)			
		3.66 (h_c)			
II-C8 (50.19)	Col_h (200)	36.41	36.41	100	*a*: 42.05
		4.69			*S* = 1531.0
		(h_a)			
	Col_h (25)	36.97	36.97	110	*a*: 42.69
		4.39			*S* = 1578.6
		(h_a)			
IIa (67.62)	Col_h (120)	43.10	43.10	100	*a*: 49.77
		24.94	24.88	110	*c* = 3.76
		16.32	16.29	210	*S* = 2145.15
		4.64			*V* = 8057.05
		(h_a)			*Z* = 1.67
		3.76 (h_c)			
	Col_h (60)	46.21	46.21	100	*a*: 53.36
		26.80	26.68	110	*c* = 3.61
		17.47	17.47	210	*S* = 2466.03
		11.62	10.60	320	*V* = 8889.30
		4.52			*Z* = 1.84
		(h_a)			
		3.61 (h_c)			
IIb (49.20)	Col_h (180)	36.67	36.67	100	*a*: 42.35
		25.85[b]	–	210	*c* = 3.75
		13.89	13.86		*S* = 1552.90
		5.0 (h_a)			*V* = 5829.64
		3.75 (h_c)			*Z* = 1.61
	Col_h (24)	37.80	37.8	100	*a*: 43.65
		18.96	18.90	200	*c* = 3.68
		14.21	14.29	210	*S* = 1649.99
		4.77			*V* = 6074.37
		(h_a)			*Z* = 1.67
		3.68 (h_c)			
IIIa (45.9)	Col_{ob} (87)	34.32	34.32	010	*a*: 41.34
		33.17	33.17	100	*b*: 42.77
		18.87	18.94	110	$\gamma = 36.65^\circ$
		17.19	17.16	020	*c* = 3.67
		16.56	16.58	200	*S* = 1768.09
		14.31	14.16	−230	*V* = 6485.87
		12.99	13.04	−310	*Z* = 2.06
		10.69	10.64	−240	
		9.69	9.85	−140	
		4.5 (h_a)			
		3.67 (h_c)			
	Col_{ob} (24)	37.28	37.28	010	*a*: 60.2
		33.94	33.94	110	*b*: 37.7
		29.77	29.77	200	$\gamma = 8.54^\circ$
		19.76	19.85	300	*c* = 3.57
		18.75	18.71	310	*S* = 2269.46

Table 2 (*continued*)

Compounds (D/Å)	Phase (*T*/°C)	d_{obs} (Å)	d_{cal} (Å)	Miller indices *hkl*	Lattice parameters (Å), lattice area *S* (Å^2), molecular volume *V* (Å^3), number of molecules in a unit cell *Z*[c]
		14.57	14.59	410	$V = 8112.63$
		17.01	16.97	220	$Z = 2.58$
		16.57	16.53	−310	
		12.91	12.68	−320	
		11.64	11.82	−130	
		10.9	10.91	−230	
		9.75	9.89	−330	
		9.35	9.32	040	
		4.40 (h_a)			
		3.57 (h_c)			
IIIb (53.58)	Col_h (100)	37.66	37.66	100	*a*: 43.49
		21.68	21.75	110	*S* = 1638.04
		4.64 (h_a)			
IIIc (70.94)	Col_r (75)	43.10	43.10	100	*a*: 43.10
		39.97	39.97	010	*b*: 39.97
		4.61 (h_a)			*S* = 1722.69

[a] The diameter (D) of the polycatenar (estimated from Chem 3D Pro 8.0 molecular model software from Cambridge Soft). d_{obs}: spacing observed; d_{cal}: spacing calculated (deduced from the lattice parameters: *a* for the Col_h phase; *a* and *b* for the Col_r and Col_{ob} phase; γ is the column tilt angle). The spacings marked h_a and h_c correspond to diffuse halos in the wide-angle region arising from correlations between the alkyl chains and core regions, respectively.

[b] Diffused peak.

[c] *Z* was calculated only when a relatively strong reflection is observed corresponding to the core–core stacking.

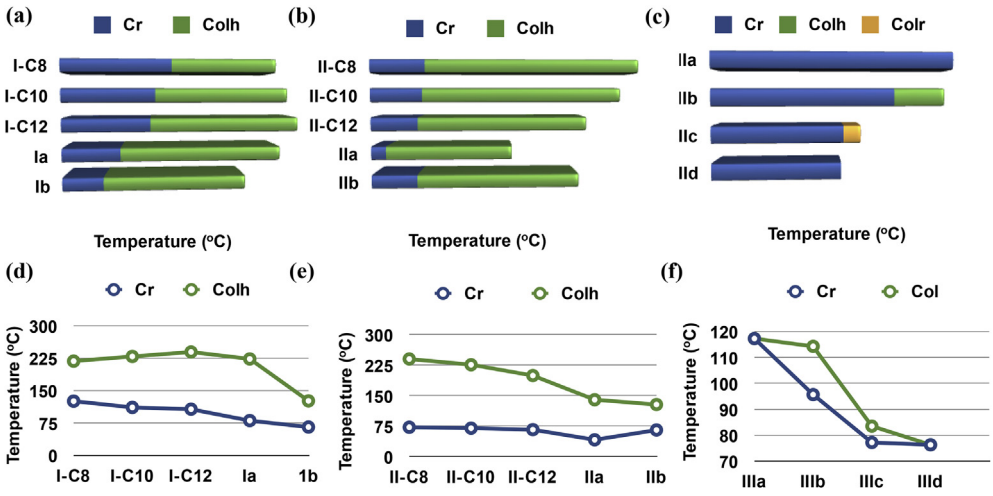

Fig. 2. Bargraph summarizing the thermal behavior (heating cycle) of stilbene based TSANs with lower homologues (a), (b) and (c); the dependence of transition temperatures on number and pattern of substitution of peripheral alkoxy tails for stilbene based TSANs (d), (e) and (f).

compounds of this series show Col phases of different symmetry as explained below.

Monotropic Col phase of compound **IIIa** under polarizing optical microscope showed a mosaic texture (Fig. 7a). The mesophase on XRD investigation showed many sharp peaks in the low angle region with two diffuse peaks in the wide-angle region, where the first one (d = 4.5 Å) corresponds to the stacking of peripheral flexible tails and the second one (d = 3.67 Å) corresponds to the stacking of disks within the column (Fig. 8a). The sharp peaks in the low angle region fits into the lattice of Col_{ob} phase with the lattice parameters a = 41.34 Å and b = 42.77 Å and column tilt angle γ = 36.6°. Enantiotropic Col phase of compound **IIIb** shows a mosaic texture in POM observations (Fig. 7b). The intensity *vs* 2θ profile extracted from the 2D X-ray diffraction pattern obtained for the Col phase of **IIIb** at 100 °C, as illustrated in Fig. 8b, shows a diffuse peak in the wide-angle region with spacing (d) of 4.6 Å indicating the liquid-like in-plane order. In the small angle region two sharp reflections with spacings of 37.7 Å and 21.7 Å were seen with the ratio of their reciprocal spacings being 1:0.58. These reflections could be indexed to (100) and (110) planes of a quasi-2D hexagonal lattice with an intercolumnar distance of 43.5 Å; Thus, the textural observation coupled with X-ray data suggests it to be a Col_h phase. There was no peak corresponding to core–core correlation. Enantiotropic Col phase exhibited by compound **IIIc** showed focal conic texture (Fig. 7c). Apparently, the identification of the LC phase on the basis of the optical texture was not clear, and thus, was investigated with the help of XRD study. XRD studies carried out at 75 °C showed two sharp peaks at low angle with d spacings of 43.1 and 39.97 Å with Miller indices (100) and (010). In the wide angle a diffused peak with a d spacing of 4.61 Å corresponds to the stacking of flexible tails. This can be indexed to a Col_r phase with lattice parameters a = 43.10 Å and b = 39.97 Å (Fig. 8c). In order to check the effect of increasing length of peripheral tails on the mesomorphic behavior, compound **IIId** was prepared. No mesomorphic

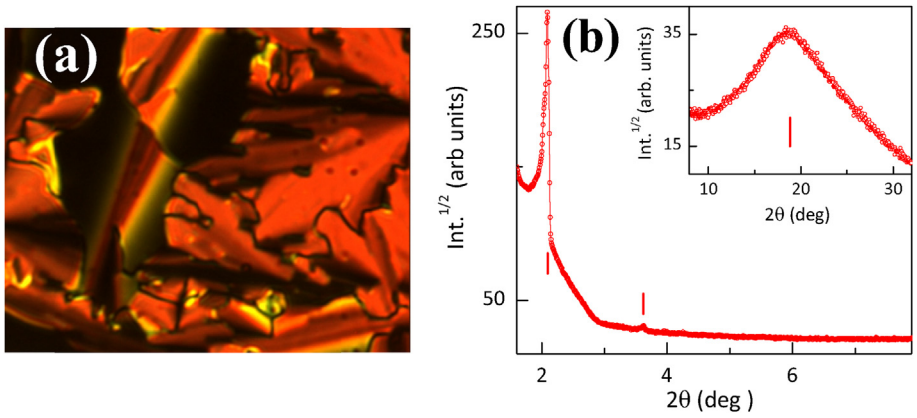

Fig. 3. Photomicrograph of the optical texture seen for the Col_h phase of **Ia** at 187 °C (a); X-ray intensity profile of the Col_h phase of TSAN **Ia** at 210 °C wherein two reflections at low angles and a diffuse peak at the wide angle region (b) can be seen.

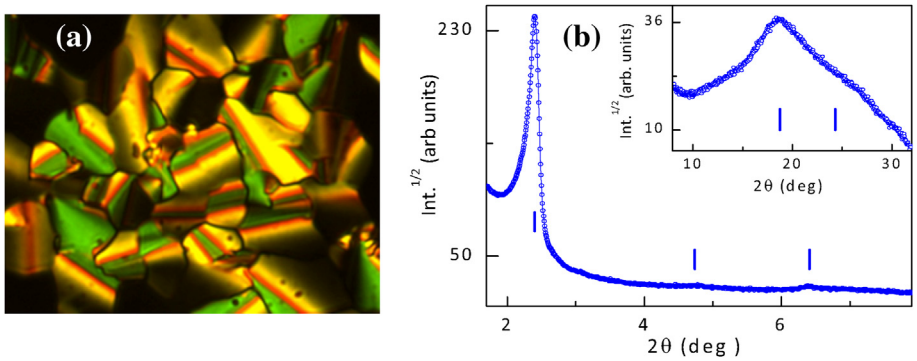

Fig. 4. Photomicrograph of the optical texture observed for Col_h phase of **Ib** at 147 °C (a); X-ray intensity *vs* 2θ profile obtained for the Col_h phase of compound **Ib** at 24 °C (b).

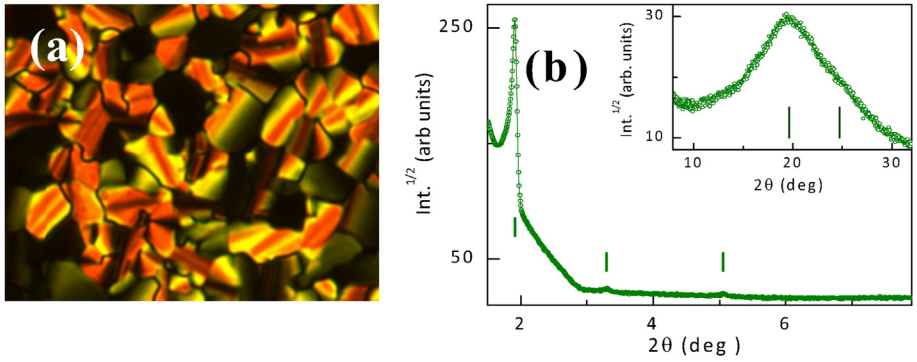

Fig. 5. Photomicrograph of optical texture obtained for Col_h phase of **IIa** at 109 °C (a); X-ray intensity profile obtained for the Col_h phase of **IIa** at 60 °C (b).

behavior was observed for this compound as evidenced by both POM and DSC studies. Thus, in this series, unlike in Series-I and II, on increasing the lengths of peripheral alkoxy tails, the mesophase range gets reduced drastically, as shown in Fig. 2c and f.

In essence, this series shows the importance of the symmetry of substitution in stabilizing Col phase. Space-filling energy minimized molecular models of representative TSANs **I-C8**, **II-C8** and **IIIa** shed some light on this aspect (Fig. 9). When compared to **I-C8** and **II-C8**, the three arms of TSAN **IIIa** are more twisted to minimize the repulsion from the alkoxy tail located in the bay region. The twist of the arms reduces the molecular planarity and as a consequence packing of discs into Col phase becomes very subtle. Thus increasing the chain length drastically affects the mesomorphic behavior in this series; either by leading to a change in the symmetry of the Col phase (as in the case of **IIIa**–**c**) or by destabilizing the Col self-assembly (as evident from the crystalline nature of **IIId**). In the case of series **I** and **II**, the pattern of peripheral alkoxy tail substitution support the Col packing and it is evidenced by the enhanced mesophase width and tendency of the mesophases to freeze in the glassy state.

2.3. Photophysical properties

As mentioned in the introduction, we expected the compounds to be emissive due to the presence of stilbene chromophores and the large delocalization of electron cloud between the peripheral region (electron donating) and the central core (electron withdrawing). We have investigated the UV–vis absorption and

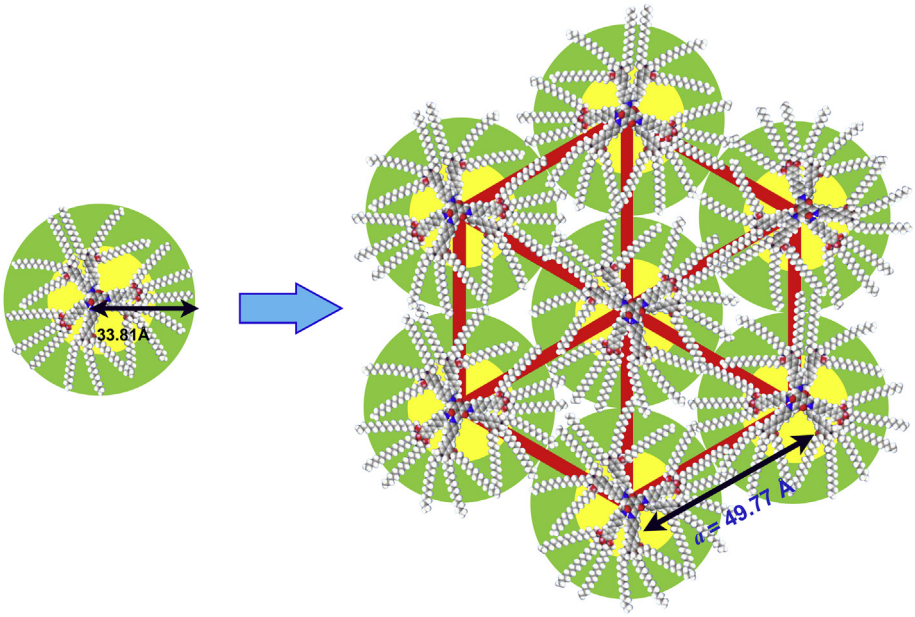

Fig. 6. Schematic showing the self-organization of compound **IIa** into hexagonal columnar (Col_h) lattice with inter-digitation of alkyl tails. Space filling energy minimized (all-*trans*) molecular model of **IIa** derived from molecular mechanics (MM2) method.

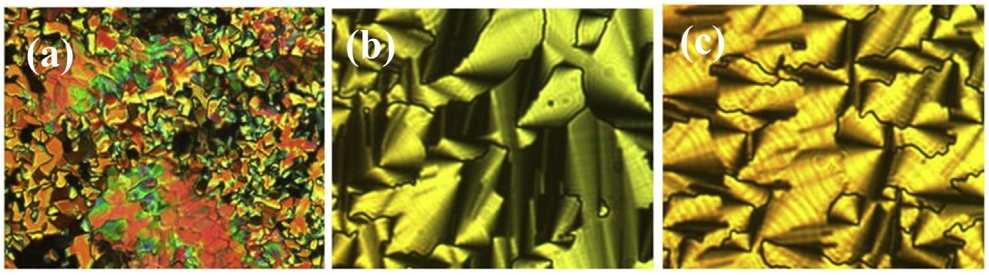

Fig. 7. Photomicrographs of optical texture obtained for Col_{ob} phase of **IIIa** at 95 °C (a); Col_h phase of **IIIb** at 83 °C (b) and Col_r phase of **IIIc** at 76 °C (c).

fluorescence behavior of one compound from each series *viz.*, **Ia**, **IIa** and **IIIc** (all with hexadecyloxy chains) in solution, solid as well as in the glassy film state. The data obtained from absorption and emission spectra of these three compounds have been summarized in Table 3. Micromolar solutions in THF, drop-cast solid and glassy films were used for the study. To begin with, the solution, solid and thin film spectra were recorded at room temperature. Solid films were prepared by drop casting the solution of the compounds in chloroform on glass coverslips and allowing the solvent to evaporate. Thin glassy films of the compounds were prepared by, sandwiching the sample between two glass coverslips and heating to the isotropic state. From the isotropic state these compounds were cooled slowly to the glassy state. As shown in the LHS portion of Fig. 10a,c and d, the absorption spectra (solid line) of all the three compounds in the solution, solid and frozen mesophase states, showed two absorption bands corresponding to $\pi-\pi^*$ and $n-\pi^*$ transitions. As expected, the absorption maxima in the solid as well as glassy state shift slightly to longer wavelength that can be ascribed to the close proximity of molecules in frozen 2D structure. Further, in comparison with short-armed TSANs [35,36], a bathochromic shift of the absorption maxima is apparent in both the states of these compounds; obviously this can be attributed to the fact that these long armed compounds with fluorophores possess an extended π-conjugation. Irradiation of these solutions (wavelength of 440 nm) yielded an intense emission with an emission maximum at around 510 nm with a negligible shoulder (Fig. 10a). There was not much difference in the absorption and emission spectra of compounds **Ia**, **IIa** and **IIIc**. The Stokes shift was found to be in the range of 65–68 nm as given in Table 3. In fact, as shown in Fig. 10b, the green emission was observed on irradiating with a light of 365 nm. The glassy films of compounds **Ia**, **IIa** and **IIIc** on exciting at the absorption maxima show a broad emission maxima, with a large Stokes shift of around 116–137 nm (see right hand side portion of Fig. 10d). This large red shift can be attributed to the aggregation of molecules leading to strong intermolecular interactions. It should be noted that, there is a less red shifted emission in the case of glassy films of compound **IIIc**, when compared to the glassy films of **Ia** and **IIa**. This may be due to the less efficient packing of molecules because of the unsymmetrical peripheral substitution in series **III** (Fig. 8). The fluorescence intensity decreased with the increase in the temperature, which is due to the breaking-up of these aggregates and thermally activated radiationless processes (See SI) [60,61]. Drop-cast films also exhibited emission spectra similar to those of glassy films (Fig. 10c). The emissive frozen Col phase of TSANs is technologically important as it possess 2D order and short intra columnar distance, which supports the charge carrier mobility with a simultaneous restriction on the mobility of ionic impurities [62]. Relative quantum yields of these compounds in solution were measured with respect to tetrakis(octyl)-1*H*-

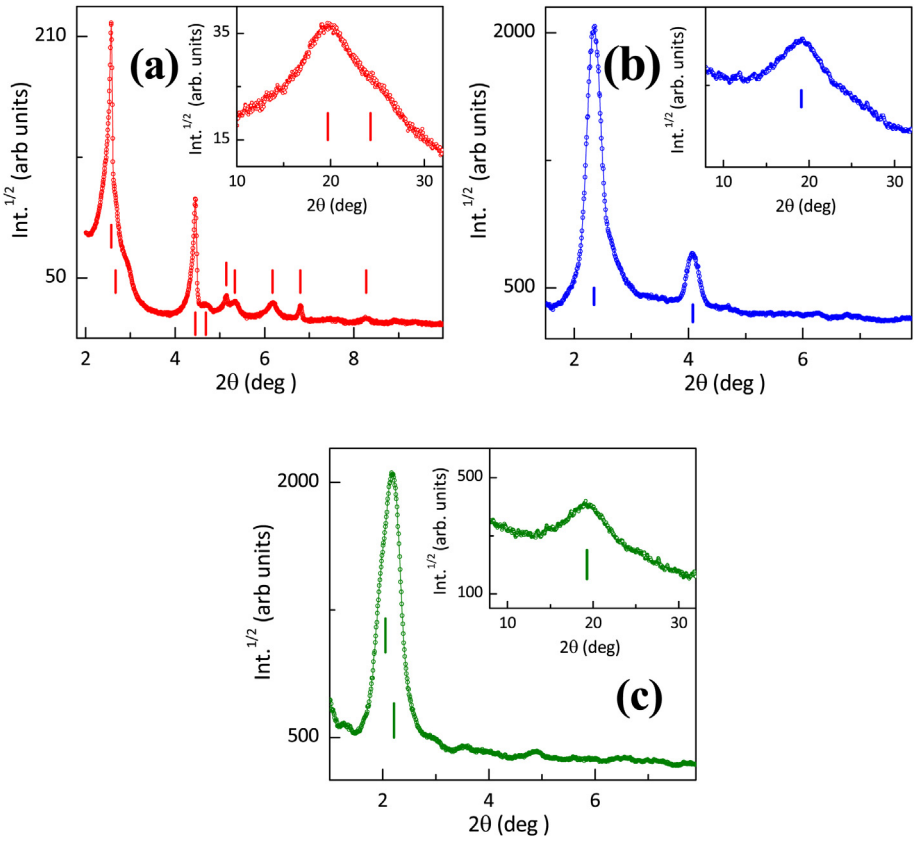

Fig. 8. The intensity *vs* 2θ profiles obtained for Col_{ob} phase of TSAN **IIIa** at 87 °C (a); Col_h phase of **IIIb** at 100 °C (b); Col_r phase of **IIIc** at 75 °C (c).

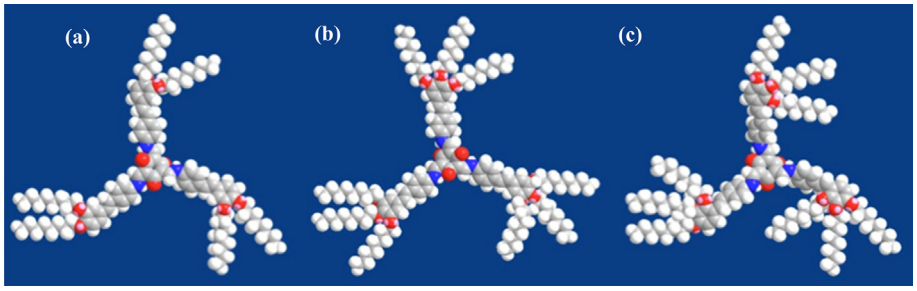

Fig. 9. Space-filling energy minimized (all-*trans*) molecular models of TSANs (a) **I-C8**; (b) **II-C8**; (c) **IIIa** derived from the molecular mechanics (MM2) method.

Table 3
Photophysical properties of luminescent TSANs.

Compound	THF solution[a]			Drop cast solid film			Glassy film		
	Absorption[b]	Emission[b,c]	Stokes shift[b]	Absorption[b]	Emission[b,c]	Stokes shift[b]	Absorption[b]	Emission[b,c]	Stokes shift[b]
Ia	353, 442	510	68	384, 443	579	136	374, 441	578	137
IIa	353, 440	505	65	379, 440	563	121	370, 441	567	126
IIIc	351, 441	508	67	387, 441	553	112	372, 441	557	116

[a] Micromolar solutions in THF.
[b] Wavelengths (nm).
[c] The excitation wavelength λ_{ex} = 440 nm.

phenanthro[1,10,9,8]carbazole-3,4,9,10-tetracarboxylate [64], and found to be in the range of 0.29–0.31 (See SI) irrespective of the substitution pattern. However, detailed investigations addressing the development of well-aligned films, annealing, film morphology, luminescence efficiency, electroluminescence, solvent effects etc. are required to go for a device fabrication.

2.4. Electrochemical properties

Cyclic voltammetry (CV) gives valuable information and allows the estimation of HOMO and LUMO levels of the organic materials. A 0.1 M solution of tetrabutylammonium hexafluorophosphate, in acetonitrile was used as a supporting electrolyte (buffer). A

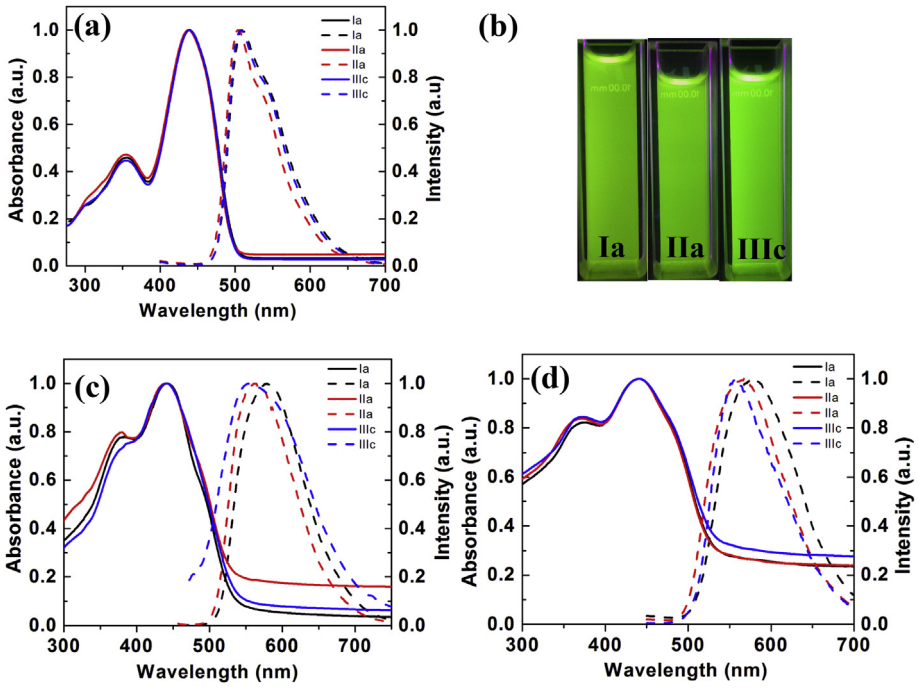

Fig. 10. Absorption (solid line) and emission spectra (dotted line) in micromolar THF solution of compounds **Ia**, **IIa** and **IIIc** (a); pictures of micromolar solutions of the same compounds on illuminating with the UV light of 365 nm (b); absorption (solid line) and emission spectra (dotted line) of drop casted films of compounds **Ia**, **IIa** and **IIIc** (c) and glassy films of the same compounds (d).

standard CV experiment by using a three-electrode cell was carried out. Specifically, a single compartment cell comprising a 1 mm diameter platinum (Pt) disc as a working electrode, a Pt wire as an auxiliary or counter electrode and saturated silver/silver chloride (Ag/AgCl) as a reference electrode, was used for the study. The reference electrode was calibrated with the ferrocene/ferrocenium (Fc/Fc^{+}) redox couple (absolute energy level of −4.80 eV to vacuum). The redox potentials of these thin-films were measured at a scanning rate of 50 mV s^{-1}. Compounds **Ia**, **IIa** and **IIIc** were chosen as representative TSANs from each series and investigated for their electrochemical behavior. The energy levels and band gaps calculated from these studies are tabulated in Table 4. The cyclic voltammograms of these compounds are given in Fig. 11. These compounds were deposited by dropping of the solutions in dichloromethane on platinum disc surface and then heated gently with hot air-gun. All the compounds exhibited well-defined irreversible oxidation and reduction waves. The optical band gap ($E_{g,opt}$) was estimated from the red edge of the absorption spectra. The HOMO–LUMO energy gap (ΔE_{CV}) value was measured from the difference in potential between oxidation and reduction and was found to be slightly different from the optical band gap, *i.e.* the value deduced from the longest wavelength absorption ($\lambda_{red\ edge}$) (Table 4) using the expression $E = h\nu$ (where $\nu = c/\lambda$). The IP (E_{HOMO}) and EA (E_{LUMO}) were determined by adding 4.7 eV (*vs* Ag/AgCl) to the oxidation and reduction potentials respectively. The values of HOMO were found to be in the range of −6.21 to −6.39 eV, whereas the values of LUMO were found to be in the range of −3.8 to −4.12 eV. The electrochemical band gaps were found to be in the range of 2.27–2.62 eV, which was comparable to the values of the optical band gaps observed (2.32–2.35 eV). The observed HOMO, LUMO levels and band gaps were lower than 1,3,5-tristyryl benzene derivative which was reported for device fabrication (HOMO: −5.71 eV; LUMO: −2.91 eV; Band gap: 2.8 eV) [65].

2.5. Atomic force microscopy studies

Atomic force microscopy (AFM) is useful tool to study the surface structures at nanometer scales and thus aids in knowing surface morphology to a large extent. We have spin coated the dichloromethane solutions of compounds **Ib**, **IIa**, **IIb** on quartz plate. These compounds were chosen because of the reason that they exhibit frozen glassy columnar phase. The topographic and phase contrast AFM images recorded for these compounds are shown in Fig. 12.

As can be seen, the topography shows a homogenous surface studded with granular structures. Further close examination of the phase contrast image (Fig. 12b,e,h) suggests the presence of long fibrils where dissimilar components show different contrasts. The root mean square (rms) roughness and thickness values of the film were found to be in the range of ~5–10 nm and 90–140 nm (±10 nm), respectively. The absorption and emission spectra were also obtained for these thin-films were found to be identical to the ones obtained for the drop casted and glassy films. Fig. 13 shows the image of these films in daylight as well as UV light of long

Table 4
Electrochemical characteristics of the representative compounds.

Compound	E_{1ox} (V)	E_{HOMO} (eV)	E_{1red} (V)	E_{LUMO} (eV)	$\Delta E_{g,CV}$ (eV)	$E_{g,opt}$ (eV)
Ia	1.51	−6.21	−0.79	−3.91	2.30	2.32
IIa	1.72	−6.42	−0.57	−3.80	2.62	2.35
IIIc	1.69	−6.39	−0.58	−4.12	2.27	2.33

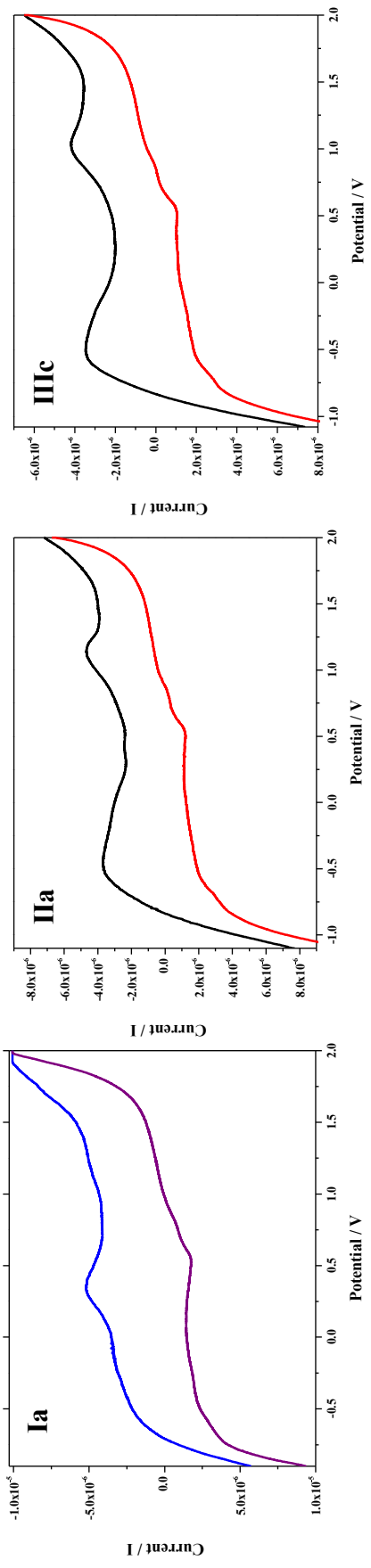

Fig. 11. Cyclic voltammograms of compounds **Ia**; **IIa** and **IIIc**.

wavelength (365 nm). From these images it is evident that emission is red shifted due to the formation of aggregates.

3. Summary

Tris(*N*-salicylideneaniline)s appended with stilbene fluorophores, which can be regarded as *pseudo*-triphenylene discotics, have been designed and synthesized. Thereby, through the incorporation of fluorophores we have examined the effects on the mesomorphic behavior and photophysical properties of discotic TSANs. Specifically, three series of stilbene-based TSANs were prepared. Of these, the first series of stilbene-based TSANs consisting of six peripheral alkoxy tails exhibit columnar behavior, and in some cases this 2D structure freezes. In this series, on increasing the chain length, the mesophase range seems to increase marginally. The second series of stilbene-based TSANs also exhibit columnar mesomorphism. In general, on increasing the chain length, both the clearing temperature and the mesophase range seem to decrease. All the members of this series freeze the columnar structure. The general trend in thermal behavior of the third series of compounds, which are the positional isomeric analogues of second series of TSANs, appear to be different; they show lower transition temperatures but seem to disfavor the mesomorphic behavior as can be seen that only the middle members with nine *n*-dodecyloxy or *n*-hexadecyloxy tails, unlike the *n*-octyloxy and *n*-octadecyloxy analogues, show enantiotropic columnar mesophase. None of these, unlike other two series of compounds, freeze the 2D structure. Symmetry of the mesophase is also very much dependent on length of the alkyl chain. The photophysical studies carried out for three representative TSANs evidenced their fluorescence characteristics in solution, mesophase, solid and glassy states. The bright green light emission was observed in the solution state. As expected, the emissive maxima in the solid/glassy state shift slightly to longer wavelength that can be ascribed to the close proximity of molecules in frozen 2D structure. Absorption and emission spectra of these three different series does not vary much depending on the pattern of substitution or on the length of the peripheral chain. Electrochemical studies revealed that these compounds exhibit lower HOMO, LUMO levels and band gaps in comparison to reported tristyryl benzene derivatives. Atomic force microscopy of the spin coated films revealed a homogeneous surface studded with granular structures, which can be further optimized. In general, it is shown that by varying the nature (polarity) of fluorophore and peripheral alkoxy chain substitution patterns affects the co-facial and edge-on interactions among the TSAN cores, and thus mesophase behavior can be altered. Specifically, the study clearly indicates that the number, length and positions of peripheral alkoxy tails strongly affect mesomorphism with almost no effect on the photophysical property. The observed light emissive feature of the Col phase and the ability to freeze in the glassy state appear to be promising from the point of OLEDs.

4. Experimental section

4.1. General

Chemicals were obtained from Fluka, Aldrich, Lancaster and local chemical companies, and were used without any purification; solvents were dried following the standard procedures. Chromatography was performed using either silica gel (60–120, 100–200 and 230–400 mesh) or neutral aluminium oxide. For thin layer chromatography, aluminium sheets pre-coated with silica gel (Merck, Kieselgel 60, F_{254}) were employed. IR spectra were recorded on a Perkin-Elmer Spectrum 1000 FT-IR spectrometer. The spectral positions are given in wave number (cm^{-1}) unit. NMR

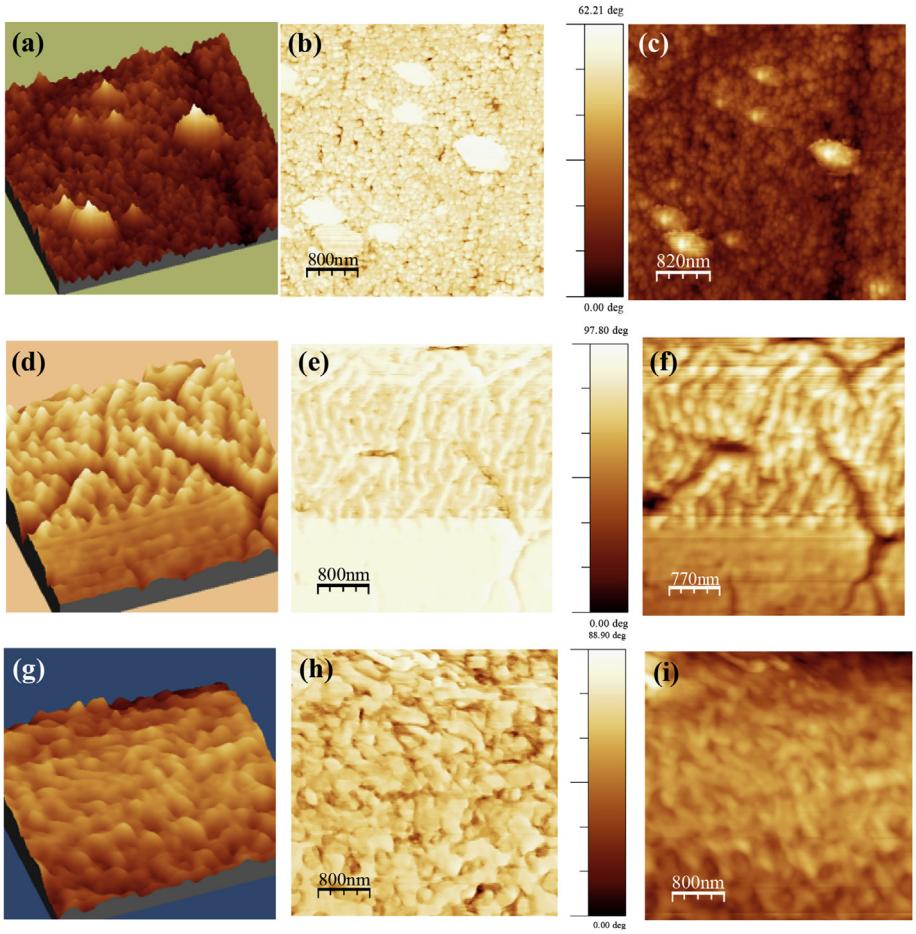

Fig. 12. Topographic AFM image, 4 μm × 4 μm in a 3D perspectives of compound **Ib** (a); compound **IIa** (d); and compound **IIb** (g); phase contrast images of compound **Ib** (b); compound **IIa** (e); and compound **IIb** (h); topography AFM images of compound **Ib** (c); compound **IIa** (f); and compound **IIb** (i).

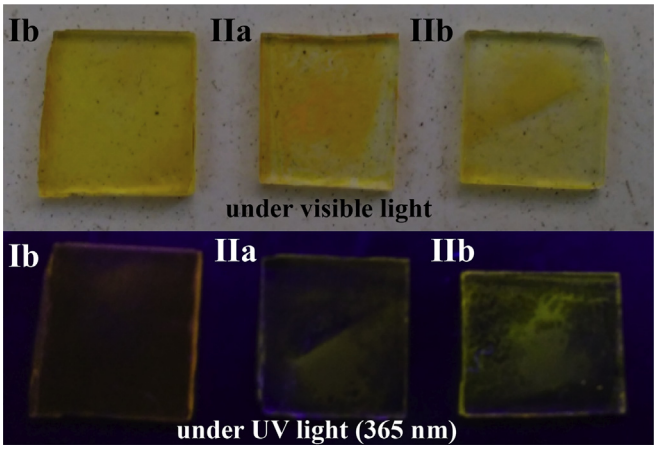

Fig. 13. Photographs of the quartz plates containing spin coated samples of compounds **Ib**, **IIa** and **IIb** under daylight (first row) and under UV light of long wavelength (365 nm) (second row).

spectra were recorded using either a Bruker DRX-500 (500 MHz) or Bruker AMX-400 (400 MHz) spectrometer or Bruker Avance series DPX-200 (200 MHz) spectrometer. For ^{1}H NMR spectra, the chemical shifts are reported in ppm relative to TMS as an internal standard. Coupling constants are in Hz. Microanalyses were performed using either a Euro EA3000 model elemental analyzer. Mass spectra were determined on JEOL JMS-600H spectrometer in FAB+ mode using 3-nitrobenzyl alcohol as a liquid matrix. Molecular length is calculated from the energy minimized structure deduced from CS Chem 3D version 9 programme. X-Ray diffraction studies were carried out on powder samples in Lindemann capillaries with CuK_{α} radiation using high-resolution powder X-ray diffractometer equipped with a focusing elliptical mirror and a high-resolution fast detector. The mesogenic compounds were investigated for their liquid crystalline behavior employing an optical polarizing microscope (Leica DMLP) equipped with a programmable hot stage (Mettler FP90) and differential scanning calorimeter (Perkin Elmer DSC7). Above mentioned optical polarizing microscope equipped with a programmable hot stage and differential scanning calorimeter were used to determine the melting points of non-mesomorphic compounds. Fluorescence emission spectra in solution state were recorded with luminescence spectrometer (Perkin Elmer LS 50B), while emission spectra as a function of temperature in solid state were obtained by using fluorolog spectrofluorimeter (SPEX) in conjunction with a programmable hot stage (Linkam). Cyclic voltammograms were recorded using a CH instruments electrochemical work station equipped with an electrochemical analyzer (CHI660E). AFM imaging was performed using an Agilent 5500 microscope; intermittent noncontact mode AFM was used for topographical characterization.

4.2. Experimental procedures and characterization data

The detailed synthetic procedures and the molecular structural

characterization data for the intermediate and target compounds are provided in the Supporting information section.

Acknowledgement

ASA sincerely thanks Science and Engineering Board (SERB), DST, Govt. of India and BRNS-DAE for funding this work through the project No. SB/S1/PC-37/2012 and No. 2012/34/31/BRNS/1039 respectively.

Appendix A. Supplementary data

Supplementary data related to this article can be found at http://dx.doi.org/10.1016/j.dyepig.2016.05.010.

References

[1] Pope M, Kallmann HP, Magnante P. Electroluminescence in organic crystals. J Chem Phys 1963;38:2042–3.
[2] Bernard V. In: Molecular fluorescence: principles and applications. Germany: Wiley-VCH; 2001.
[3] Kelly SM. In: Flat panel displays: advanced organic materials. RSC Materials Monographs (Royal Society of Chemistry); 2000.
[4] Kraft A, Grimsdale AC, Holmes AB. Electroluminescent conjugated polymers-seeing polymers in a new light. Angew Chem Int Ed 1998;37:403–28.
[5] Christ T, Glusen B, Greiner A, Kettner A, Sander R, Stumpflen V, et al. Columnar discotics for light emitting diodes. Adv Mater 1997;9:48–52.
[6] Seguy I, Destruel P, Bock H. An all-columnar bilayer light-emitting diode. Synth Met 2000;111–112:15–8.
[7] Seguy I, Jolinat P, Destruel P, Farenc J, Mamy R, Bock H, et al. Red organic light emitting device made from triphenylene hexaester and perylene tetraester. J Appl Phys 2001;89:5442–8.
[8] Hassheider T, Benning SA, Kitzerow H-S, Achard M-F, Bock H. Color-tuned electroluminescence from columnar liquid crystalline alkyl arenecarboxylates. Angew Chem Int Ed 2001;40:2060–3.
[9] (a) In: Li Q, editor. Liquid crystals beyond displays: chemistry, physics, and applications. Hoboken, New Jersey: John Wiley & Sons; 2012.
(b) Gregg BA, Fox MA, Bard AJ. Photovoltaic effect in symmetrical cells of a liquid crystal porphyrin. J Phys Chem 1990;94:1586–98.
[10] (a) Sun Q, Dai L, Zhou X, Li L, Li Q. Bilayer- and bulk-heterojunction solar cells using liquid crystalline porphyrins as donors by solution processing. Appl Phys Lett 2007;91:253505/1–253505/3.
(b) Zhou X, Kang S-W, Kumar S, Kulkarni RR, Cheng SZD, Li Q. Self-assembly of porphyrin and fullerene supramolecular complex into highly ordered nanostructure by simple thermal annealing. Chem Mater 2008;20:3551–3.
(c) Zhou X, Kang S-W, Kumar S, Li Q. Self-assembly of discotic liquid crystal porphyrin into more controllable ordered nanostructure mediated by fluorophobic effect. Liq Cryst 2009;36(3):269–74.
[11] Li L, Kang S-W, Harden J, Sun Q, Zhou X, Dai L, et al. Nature-inspired light-harvesting liquid crystalline porphyrins for organic photovoltaics. Liq Cryst 2008;35:233–9.
[12] Cherian S, Donley C, Mathine D, LaRussa L, Xia W, Armstrong N. Effects of field dependent mobility and contact barriers on liquid crystalline phthalocyanine organic transistors. J Appl Phys 2004;96:5638–43.
[13] Tatemichi S, Ichikawa M, Koyama T, Taniguchi Y. High mobility n-type thin-film transistors based on N,N′-ditridecyl perylene diimide with thermal treatments. Appl Phys Lett 2006;89:112108/1–112108/3.
[14] Schmidt R, Oh JH, Sun Y-S, Deppisch M, Krause A-M, Radacki K, et al. High-performance air-stable n-channel organic thin film transistors based on halogenated perylene bisimide semiconductors. J Am Chem Soc 2009;131:6215–28.
[15] Majumdar KC, De N, Roy B, Bhaumik A. Synthesis and mesophase characterization of a series of new triazine-based disc-shaped molecules. Liq Cryst 2010;37:1459–64.
[16] Kohlmeier A, Vogel L, Janietz D. Multiple hydrogen bonded mesomorphic complexes between complementary 1,3,5-triazine and pyrimidine derivatives. Soft Matter 2013;9:9476–86.
[17] Castelar S, Barberá J, Marcos M, Romero P, Serrano J-L, Golemme A, et al. Supramolecular dendrimers based on the self-assembly of carbazole-derived dendrons and triazine rings: liquid crystal, photophysical and electrochemical properties. J Mater Chem C 2013;1:7321–32.
[18] Boden N, Bushby RJ, Lozman OR. Designing better columnar mesophases. Mol Cryst Liq Cryst 2003;400:105–13.
[19] Bushby RJ, Hamley IW, Liu Q, Lozman OR, Lydon JE. Self-assembled columns of fullerene. J Mater Chem 2005;15:4429–34.
[20] Gearba RI, Lehmann M, Levin J, Ivanov DA, Koch MHJ, Barbera J, et al. Tailoring discotic mesophases: columnar order enforced with hydrogen bonds. Adv Mater 2003;15:1614–8.
[21] Chang T-H, Wu B-Ru, Chiang MY, Liao S-C, Ong CW, Hsu H-F, et al. Synthesis and mesomorphic behavior of a donor-acceptor-type hexaazatriphenylene. Org Lett 2005;7:4075–8.
[22] Clark J, Archer R, Redding T, Foden C, Tant J, Geerts Y, et al. Charge recombination in distributed heterostructures of semiconductor discotic and polymeric materials. J Appl Phys 2008;103:124510/1–124510/6.
[23] Ecoffet C, Markovitski D, Jallabert C, Strzelecka H, Veber M. Columnar liquid crystals of triaryl pyrylium salts: experimental and theoretical study of photophysical properties. Thin Solid Films 1994;242(1–2):83–7.
[24] Marguet S, Markovitski D, Goldmann D, Janietz D, Praefcke K, Singer D. Spectroscopic properties of nematic discotic phenylethynylbenzene derivatives: symmetry effects. J Chem Soc Faraday Trans 1997;93:147–55.
[25] Cormierand RA, Gregg BA. Synthesis and characterization of liquid crystalline perylene diimides. Chem Mater 1998;10:1309–19.
[26] Rohr U, Schlichting P, Bohm A, Gross M, Meerholz K, Brauchleand C, et al. Liquid crystalline coronene derivatives with extraordinary fluorescence properties. Angew Chem Int Ed 1998;37:1434–7.
[27] Ito S, Herwig PT, Bohme T, Rabe JP, Rettig W, Mullen K. Bishexa-peri-hexabenzocoronenyl: a “Superbiphenyl”. J Am Chem Soc 2000;122:7698–706.
[28] Benning SA, Hassheider T, Keuker-Bauman S, Bock H, Salla FD, Frauenheim T, et al. Absorption and luminescence spectra of electroluminescent liquid crystals with triphenylene, pyrene and perylene units. Liq Cryst 2001;28:1105–13.
[29] Attias AJ, Cavalli C, Donnio B, Guillon D, Hapiot P, Malthete J. Columnar mesophase from a new disc like mesogen based on a 3,5-dicyano-2,4,6-tristyrylpyridine core. Chem Mater 2002;14:375–84.
[30] Kulkarni AP, Tonzola CJ, Babel A, Jenekhe SA. Electron transport materials for organic light-emitting diodes. Chem Mater 2004;16:4556–73.
[31] Chong JH, Sauer M, Patrick BO, MacLachlan MJ. Highly stable keto-enamine salicylideneanilines. Org Lett 2003;5:3823–6.
[32] Sauer M, Yeung C, Chong JH, Patrick BO, MacLachlan MJ. N-Salicylideneanilines: tautomers for formation of hydrogen-bonded capsules, clefts, and chains. J Org Chem 2006;71:775–88.
[33] Yelamaggad CV, Achalkumar AS, Rao DSS, Prasad SK. Self-assembly of C(3)(h) and C(s) symmetric keto-enamine forms of tris(N-salicyl-ideneanilines) into columnar phases: a new family of discotic liquid crystals. J Am Chem Soc 2004;126:6506–7.
[34] Yelamaggadand CV, Achalkumar AS. Tris(N-salicylideneanilines) [TSANs] exhibiting a room temperature columnar mesophase: synthesis and characterization. Tetrahedron Lett 2006;47:7071–5.
[35] Yelamaggad CV, Achalkumar AS, Rao DSS, Prasad SK. The first examples of optically active tris(N-salicylideneaniline)s: manifestation of chirality from molecules to fluid columnar phases. J Mater Chem 2007;17:4521–9.
[36] Yelamaggad CV, Achalkumar AS, Rao DSS, Prasad SKA. New class of discotic mesogens derived from tris(N-salicylideneaniline)s existing in C_{3h} and C_s keto-enamine forms. J Org Chem 2007;72:8308–18.
[37] Yelamaggad CV, Achalkumar AS, Rao DSS, Prasad SK. Luminescent, liquid crystalline tris(N-salicylideneaniline)s: synthesis and characterization. J Org Chem 2009;74:3168–71.
[38] Yelamaggad CV, Achalkumar AS. Light emitting, star-shaped tris(*N*-salicylideneaniline) discotic liquid crystals bearing *trans*-stilbene fluorophores: synthesis and characterization. Tetrahedron Lett 2012;53:7108–12.
[39] Achalkumar AS, Hiremath US, Rao DSS, Prasad SK, Yelamaggad CV. Self-assembly of hekates-tris(*N*-salicylideneaniline)s into columnar structures: synthesis and characterization. J Org Chem 2013;78:527–44.
[40] Riddle JA, Bollinger JC, Lee D. Escape from a nonporous solid: mechanically coupled biconcave molecules. Angew Chem Int Ed 2005;44:6689–93.
[41] Riddle JA, Lathrop SP, Bollinger JC, Lee D. Schiff base route to stackable pseudo-triphenylenes: stereoelectronic control of assembly and luminescence. J Am Chem Soc 2006;128:10986–7.
[42] Jiang X, Bollinger JC, Lee D. Two-dimensional electronic conjugation: cooperative folding and fluorescence switching. J Am Chem Soc 2006;128:11732–3.
[43] Hayer A, de Halleux V, Kohler A, El-Garoughy A, Meijer EW, Barbera J, et al. J Phys Chem B 2006;110:7653–9.
[44] Meier H. The photochemistry of stilbenoid compounds and their role in materials technology. Angew Chem Int Ed 1992;31:1399–420.
[45] Lehmann M, Kohn C, Meir H, Renker S, Oehlhof A. Supramolecular order of stilbenoid dendrons: importance of weak interactions. J Mater Chem 2006;16:441–51.
[46] Burroughes JH, Bradeley DDC, Brown AR, Marks RN, Mackay K, Friend RH, et al. Light-emitting diodes based on conjugated polymers. Nature 1990;347:539–41.
[47] Gustafsson G, Cao Y, Treacy GM, Klavetter F, Burn PL, Burroughes JH, et al. Photoluminescence and electroluminescence in conjugated polymeric systems. Synth Met 1993;55–57:4031–40.
[48] Yu G, Wang J, McElvain J, Heeger AJ. Large-area, full-color image sensors made with semiconducting polymers. Adv Mater 1998;10:1431–4.
[49] Piok T, Brands C, Neyman PJ, Earlacher A, Soman C, Murray MA, et al. Photovoltaic cells based on ionically self-assembled nanostructures. Synth Met 2001;116:343–7.
[50] See Supporting information.
[51] Barbera J, Gimenez R, Serrano JL. Mesogenic pyrazaboles: synthesis, properties, and structural characterization. Chem Mater 2000;12:481–9. and references cited therein.
[52] Carfagna C, Roviello A, Sirigu A. Disk-like mesogens: synthesis and characterization of a series of rufigallol hexa-n-alkanoates. Mol Cryst Liq Cryst

1985;122:151–60.
[53] Gramsbergen EF, Hoving HJ, de Jeu WH, Praefcke K, Kohne B. X-ray investigation of discotic mesophases of alkylthio substituted triphenylenes. Liq Cryst 1986;1:397–400.
[54] Metersdorf H, Ringsdorf H. Self-organization of substituted azacrowns based on their discoid and amphiphilic nature. Liq Cryst 1989;5:1757–72.
[55] Zeng H, Carroll PJ, Swager TM. The development of polar discotic metallomesogens: vanadyl 1,3-diketone complexes. Liq Cryst 1993;14:1421–9.
[56] Laschat S, Baro A, Steinke N, Giesselmann F, Hagele C, Scalia G, et al. Discotic liquid crystals: from tailor-made synthesis to plastic electronics. Angew Chem Int Ed 2007;46:4832–87.
[57] Kleppinger R, Lillyaand CP, Yang C. Discotic liquid crystals through molecular self-assembly. J Am Chem Soc 1997;119:4097–102.
[58] Festag R, Kleppinger R, Soliman M, Wendorff JH, Lattermannand G, Staufer G. Supermolecular self organization via molecular aggregation. II. Electrooptical studies on structure formation processes in associated liquid-crystalline diols. Liq Cryst 1992;11:699–710.
[59] Collard DM, Lillya CP. Supermolecular self organization via molecular aggregation. II. Electrooptical studies on structure formation processes in associated liquid-crystalline diols. J Am Chem Soc 1987;109:7544–5.
[60] Birks JB. The photophysics of aromatic excimers. In: Gordon M, Ware WR, editors. The exiplex. New York: Academic Press; 1975. p 39.
[61] Duan X-F, Wang J-L, Pei J. Nanosized π-Conjugated molecules based on truxene and porphyrin: synthesis and high fluorescence quantum yields. Org Lett 2005;7:4071–4.
[62] Percec V, Glodde M, Bera TK, Miura Y, Shiyanovskaya I, Singer KD, et al. Self-organization of supramolecular helical dendrimers into complex electronic materials. Nature 2002;419:384–7.
[63] Pathak SK, Nath S, Gupta RK, Rao DSS, Prasad SK, Achalkumar AS. Effect of regioisomerism on the self-assembly and photophysical behavior of 1,3,4-thiadiazole-based polycatenars. J Mater Chem C 2015;3:8166–82.
[64] Gupta RK, Pathak SK, Pradhan B, Rao DSS, Prasad SK, Achalkumar AS. Self-assembly of luminescent *N*-annulated perylene tetraesters into fluid columnar phases. Soft Matter 2015;11:3629–36.
[65] Coya C, de Andrés A, Zaldo C, Álvarez AL, Arredondo B, Gómez R, et al. Full-solution-processed blue organic light emitting device based on a fluorescent 1,3,5-tristyrylbenzene stilbenoid small molecule. J Appl Phys 2009;105:044510.